International Journal of Engineering and Advanced Technology (IJEAT)
ISSN: 2249-8958 (Online), Volume-7 Issue-1, October 2017

Modeling and Control of Inversely Connected Rotors of Brushless Doubly Fed Twin Stator Induction Generator

A. Mahdy, S. M. EL-Hakim, M. Abdel Hakim

Abstract*: This paper presents a steady state and dynamic modeling of inversely connected rotors of Brushless Doubly Fed Twin Stator Induction Generator (BDFTSIG). The BDFTSIG consists of two identical machines, one is called power machine whose stator is connected directly to the grid and the other machine is called control machine whose stator is connected to a pulse width modulation converters. A vector control scheme is applied on the grid side converter (GSC) to control the DC link bus voltage; another vector control scheme is applied on the control machine side converter (CMSC) for synchronization and also to control the active and reactive power delivered to the grid. The system is simulated using MATLAB/Simulink environment. The simulation results show a good performance comparing with conventional doubly fed induction generator, under various loading and rotor speed conditions.

***Keywords*: BDFTSIG, vector control, inversely connected rotors.**

Subscripts sp, sc, rc, rp	*PM & CM stators and rotors*
Subscripts d,q,g	*d-axis & q-axis, grid*
ω_m	*Mechanical angular speed in rad/s*
p	*Pole pair*
s	*Slip*
L_l, L_m	*Leakage & mutual Inductance in H*
T_e	*Electromagnetic torques in N.m*
P_{wind}	*Mechanical wind power in watt*
V_{wind}	*Wind velocity in m/s*
ρ	*Air density in kg/m^3*
C_p	*Wind power coefficient*
λ	*Tip speed ratio*
ω_T	*Turbine angular speed in rad/s*
R_T	*Turbine rotor radius in meter*
E	*DC-link voltage in volt*
θ	*Orientation angular position in rad*
φ	*Magnetic Flux in webers*
P, Q	*Active & reactive power in watt, VAR*

I. INTRODUCTION

Nowadays there is a huge increase in demand and relying on renewable energy resources as an alternative for traditional fossil fuel energy resources.

Manuscript published on 30 October 2017.
***** Correspondence Author (s)
A. Mahdy*, Teaching assistant in Electrical Power & Machines Dept., Faculty of Engineering, Cairo University, Egypt, E-mail: amro_nasr@yahoo.com
S. M. EL-Hakim, Professor in Electrical Power & Machines Dept., Faculty of Engineering, Cairo University, Egypt, E-mail: smhakime@yahoo.com
M. Abdel Hakim, Professor at Electrical Power & Machines Dept., Faculty of Engineering, Cairo University, Egypt, E-mail: mhakim4545@gmail.com

© The Authors. Published by Blue Eyes Intelligence Engineering and Sciences Publication (BEIESP). This is an open access article under the CC-BY-NC-ND license http://creativecommons.org/licenses/by-nc-nd/4.0/

A Doubly Fed Induction Generator (DFIG) has a significant advantage in high power wind energy conversion systems (WECS), Because of possible independent control of the active and reactive power that can be achieved by using a power electronic converter connected to the rotor side circuit, which handles only a fraction of the total delivered power making them suitable for wind power applications. The main disadvantage of the DFIG is the existence of slip rings and carbon brushes, carbon brushes are known to have limited life span and therefore are replaced every couple of months result in an increases the maintenance costs due to wearing and depreciation, also carbon dust is conducting in nature and when trapped in the generator windings it will increase the risk of sparking between the winding conductors which could result in the weakening of the insulation and therefore a reduction of system reliability [1-3], to overcome this drawback a Brushless DFIG is used instead, the BDFIG are without brushes and slip rings and hence achieving higher reliability and lower maintenance cost. A BDFIG consists of two stator windings with different number of poles located in a single frame, those stators are magnetically coupled and electrically insulated, this type of machines have a common shaft with a special type of rotor "nested-loop" design. The first stator winding (power winding) is directly connected to the grid while the second stator winding (control winding) is connected to the grid through a controlled power converter [4-9]. Another equivalent alternative scheme is used for the BDFIG which is the BDFTSIG which consists of twin slip ring type induction machines. One of the two machines whose stator is connected directly to the grid is called a power machine (PM), while the other machine whose stator is connected to a power converter is called a control machine (CM), in this scheme the two rotors mechanically coupled and direct electrically connected through rotor circuits. The rotor terminals have two possibilities of connections, the first connection is back to back / positive sequence connection, Duro Basic et al. presented a study for the transient performance of BDFTSIG under vector control for this type of rotors connection [10], the second connection is a negative / inverse sequence connection which is more preferable as it ensures that the generated torques act in the same direction and the resultant torques is the summation of both machines' produced torques, Duro Basic et al. presented a study for steady state performance and modeling of BDFTSIG for this type of rotor connection [11], similarly Marek Adamowicz et al. presented a study for the steady state analysis [12], also Zohier et al. presented a study for the dynamic and steady state performance [13].

© Copyright: All rights reserved.

A control schemes were presented for back to back rotors connection, Kostyantyn Protsenko et al. presented a control scheme for active and reactive power control by means of a four quadrant power converter under the closed-loop stator flux oriented control scheme for back to back sequence rotors connection [14], also A. Bensadeq et al. presented an indirect vector control for grid operation of a BDFTSIG to control the power flow into the grid with a variable speed prime mover such as a wind turbine [15].

In this paper both steady state and dynamic model is presented for inversely rotor directly connected BDFTSIG system shown in Fig. 1. A vector control scheme is used to control the DC link bus at unity power factor using a PI controlled grid side converter (GSC) which is connected to the grid, another vector control scheme is used for the synchronization with the grid, and for achieving active and reactive power control using a PI controlled machine side converter (CMSC) which achieves a good transient response. Both vector control schemes are validated and the dynamic performance results are represented and analyzed by using MATLAB/Simulink environment. The results show a good performance under various loading and rotor speed conditions.

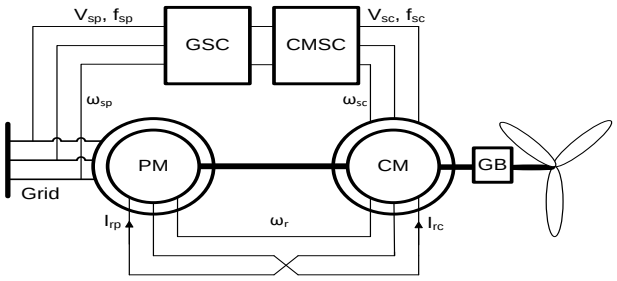

Fig. 1 Inverse sequence rotor connected BDFTSIG

II. MATHEMATICAL MODELING OF BDFTSIG

A. Mode of Operation

A BDFTSIG can operate in several ways but the synchronous mode is used for controlled variable-speed operation [5&13]. When the BDFTSIG operates in synchronous mode, there is a single frequency of current in the rotor, which is given by:

$$\omega_{rp} = \omega_{sp} - p_p\,\omega_m \qquad (1)$$

$$\omega_{rc} = \omega_{sc} - p_c\,\omega_m \qquad (2)$$

Accordingly the slips for the two machines are given by:

$$s_p = \frac{\omega_{rp}}{\omega_{sp}} = \frac{\omega_{sp} - p_p\,\omega_m}{\omega_{sp}} \qquad (3)$$

$$s_c = \frac{\omega_{rc}}{\omega_{sc}} = \frac{\omega_{sc} - p_c\,\omega_m}{\omega_{sc}} \qquad (4)$$

To produce constant torque the cross-coupling condition should be satisfied, which is:

$$\omega_{rp} = -\,\omega_{rc} \qquad (5)$$

$$\omega_{sp} - p_p\,\omega_m = -\,\omega_{sc} + p_c\,\omega_m \qquad (6)$$

$$\omega_{sc} = (p_p + p_c)\,\omega_m - \omega_{sp} \qquad (7)$$

From (3), (4) and (5) we can deduce the relation between PM and CM slips and frequencies from the following equation:

$$\frac{s_p}{s_c} = -\frac{\omega_{sc}}{\omega_{sp}} \qquad (8)$$

The synchronous speed of the BDFTSIG is half the synchronous speed of the both machines, leading to a shaft angular velocity is given by:

$$\omega_m = \frac{\omega_{sp} + \omega_{sc}}{p_p + p_c} \qquad (9)$$

A. Dynamic Modeling of BDFTSIG

The mathematical dynamic model of the BDFTSIG can be derived from the models of two slip ring induction machines with inversely connected rotors as shown in fig. 1. This dynamic model is represented in two-phase coordinates (dq) rotating at synchronous speed in the matrix form as given in (10), for derivation see appendix.

B. Steady State Modeling of BDFTSIG

The steady state per-phase equivalent circuit of BDFTSIG after referring to stator winding of PM is shown in Fig. 2. The BDFTSIG steady states per phase modeling equations are as follows:

$$\begin{bmatrix} V_{sp} \\ 0 \\ V_{sc} \end{bmatrix} = \begin{bmatrix} R_{sp} + j\,\omega_{sp}\,L_{sp} & j\,\omega_{sp}\,L_m & 0 \\ j\,\omega_{sp}\,L_m & R_r/s_p + j\,\omega_{sp}\,L_r & -j\,\omega_{sp}\,L_m \\ 0 & -j\frac{s_p}{s_c}\,\omega_{sp}\,L_m & R_{sc} + j\frac{s_p}{s_c}\,\omega_{sp}\,L_{sc} \end{bmatrix} * \begin{bmatrix} I_{sp} \\ I_r \\ I_{sc} \end{bmatrix} \qquad (11)$$

Neglecting the saturation effect ($L_{mp} = L_{mc} = L_m$), $L_{sp} = L_{lsp} + L_{mp}$, $L_{sc} = L_{lsc} + L_{mc}$, $L_{rp} = L_{lrp} + L_{mp}$, $L_{rc} = L_{lrc} + L_{mc}$, because the two machines are assumed to be identical, R_r is the sum of rotor resistances $R_r = R_{rp} + R_{rc}$ and L_{lr} is the sum of rotor leakage inductances $L_{lr} = L_{lrp} + L_{lrc}$.

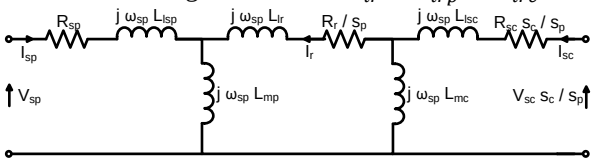

Fig. 2 Steady state per phase eq. circuit of BDFTSIG

The electromagnetic torque equation is given by:

$$T_{ep} = \frac{3}{2}p_p\,L_{mp}\,im\{i_{sp}\,i_{rp}^*\} = \frac{3}{2}p_p\,L_{mp}\,im\{i_{sp} * i_r\} \qquad (12)$$

$$T_{ec} = \frac{3}{2}p_c\,L_{mc}\,im\{i_{sc}\,i_{rc}^*\} = \frac{3}{2}p_c\,L_{mc}\,im\{i_{sc} * i_r\} \qquad (13)$$

$$T_e = T_{ep} + T_{ec} \qquad (14)$$

$$\begin{bmatrix} V_{qsp} \\ V_{dsp} \\ 0 \\ 0 \\ V_{qsc} \\ V_{dsc} \end{bmatrix} = \begin{bmatrix} (R_{sp}+SL_{sp}) & \omega_{sp}L_{sp} & SL_{mp} & \omega_{sp}L_{mp} & 0 & 0 \\ -\omega_{sp}L_{sp} & (R_{sp}+SL_{sp}) & -\omega_{sp}L_{mp} & SL_{mp} & 0 & 0 \\ SL_{mp} & (\omega_{sp}-p_p\omega_m)L_{mp} & (R_r+SL_r) & (\omega_{sp}-p_p\omega_m)L_r & -SL_{mc} & (\omega_{sp}-p_p\omega_m)L_{mc} \\ -(\omega_{sp}-p_p\omega_m)L_{mp} & SL_{mp} & -(\omega_{sp}-p_p\omega_m)L_r & (R_r+SL_r) & (\omega_{sp}-p_p\omega_m)L_{mc} & SL_{mc} \\ 0 & 0 & -SL_{mc} & \left((p_p+p_c)\omega_m-\omega_{sp}\right)L_{mc} & (R_{sc}+SL_{sc}) & \left((p_p+p_c)\omega_m-\omega_{sp}\right)L_{sc} \\ 0 & 0 & \left((p_p+p_c)\omega_m-\omega_{sp}\right)L_{mc} & SL_{mc} & -\left((p_p+p_c)\omega_m-\omega_{sp}\right)L_{sc} & (R_{sc}+SL_{sc}) \end{bmatrix} * \begin{bmatrix} i_{qsp} \\ i_{dsp} \\ i_{qr} \\ i_{dr} \\ i_{qsc} \\ i_{dsc} \end{bmatrix} \qquad (10)$$

Published By:
Blue Eyes Intelligence Engineering
and Sciences Publication (BEIESP)
© Copyright: All rights reserved.

III. CONTROLLING OF BDGTSIG SYSTEM

A. Grid Side Converter Controller

The main purpose of GSC is to regulate the voltage of the DC bus regardless of the magnitude and direction of CM power flow. Moreover, it is allowed to generate or absorb reactive power for voltage support requirements. This function is realized with a stator field oriented vector control scheme which enables the decoupled control of active and reactive power flowing between the three-phase grid and the GSC through the PWM converter. Fig.3 shows the connection arrangement of the GSC. The relationship of the inductance and resistance in fig. 3, the voltage equations can be written as follows:

$$\begin{bmatrix} v_{ag} \\ v_{bg} \\ v_{cg} \end{bmatrix} = R \begin{bmatrix} i_{ag} \\ i_{bg} \\ i_{cg} \end{bmatrix} + L \frac{d}{dt} \begin{bmatrix} i_{ag} \\ i_{bg} \\ i_{cg} \end{bmatrix} + \begin{bmatrix} v_{a1} \\ v_{b1} \\ v_{c1} \end{bmatrix} \quad (15)$$

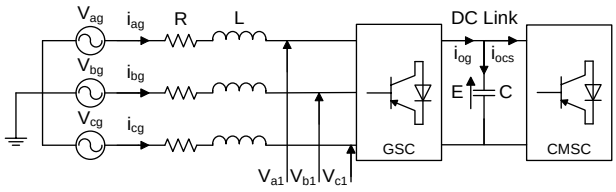

Fig. 3 GSC connection arrangement

The voltages equations in (15) can be rewritten in synchronously rotating *dq*-axis reference frame as follows:

$$v_{dg} = R\, i_{dg} + L \frac{di_{dg}}{dt} - \omega_{sp} L\, i_{qg} + v_{d1} \quad (16)$$

$$v_{qg} = R\, i_{qg} + L \frac{di_{qg}}{dt} + \omega_{sp} L\, i_{dg} + v_{q1} \quad (17)$$

Where R and L are the supply side impedance components, the active and reactive power to/from the grid equations can be written in synchronously rotating *dq*-axis reference frame as follows:

$$P_g = \frac{3}{2}(v_{dg}\, i_{dg} + v_{qg}\, i_{qg}) \quad (18)$$

$$Q_g = \frac{3}{2}(v_{qg}\, i_{dg} - v_{dg}\, i_{qg}) \quad (19)$$

For decoupled control of grid side converter (GSC), the supply voltage angular position is given by:

$$\theta_{sp} = \int \omega_{sp}\, dt = tan^{-1} \frac{v_\beta}{v_\alpha} \quad (20)$$

Where v_β and v_α are the stationary axis frame for the grid side voltage. By aligning the synchronously rotating *d*-axis reference frame with the grid side angle this will result in $v_{qg} = 0$ and since the amplitude of the supply voltage is constant, v_{dg} will be constant too, so the active and reactive power to/from the grid in (18) & (19) can be rewritten in synchronously rotating *dq*-axis reference frame as follows:

$$P_g = \frac{3}{2}\, v_{dg}\, i_{dg} \quad (21)$$

$$Q_g = -\frac{3}{2}\, v_{dg}\, i_{qg} \quad (22)$$

(21) & (22) demonstrate that the active and re-active powers from the grid-side converter are controlled via i_{dg} and i_{qg} components of current respectively. The vector control scheme is implemented using two control loops: an *outer* voltage control loop consisting of a DC voltage regulator. The output of the DC voltage regulator is the reference current i_d^* for the current regulator which regulates the PWM converter. The *inner* current control loop consists of a current regulator controlling the magnitude and phase of the voltage generated by converter from the i_d^* reference and a specified *q*-axis i_q^* reference regulating the reactive power similarly as [16-20]. The reference values for the GSC can be written as:

$$v_{d1}^* = -v_d' + (\omega_{ps} L\, i_{qg} + v_{d1}) \quad (23)$$

$$v_{q1}^* = -v_q' - (\omega_{ps} L\, i_{dg}) \quad (24)$$

Where the reference voltage v_{d1}^* and v_{q1}^* are the reference values for the final PWM signal generation for the converter IGBT switching of the GSC, and the terms between brackets are the voltage compensation terms. The voltage compensated terms make it possible to achieve decoupled control using vector control of the GSC converter. Fig. 4 shows the block diagram for the vector control of GSC.

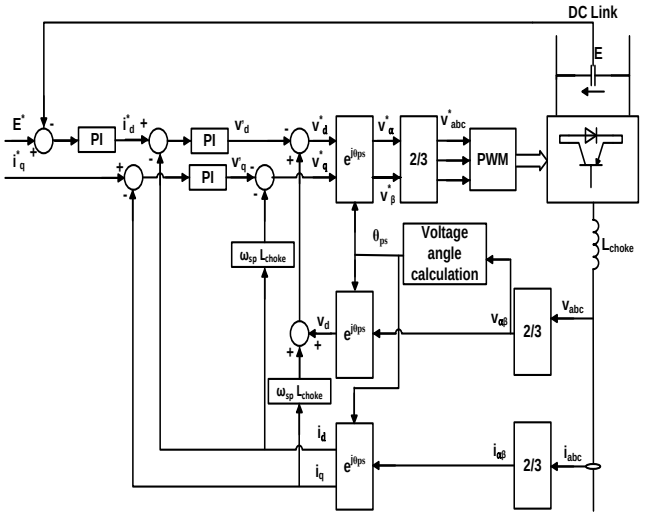

Fig. 4 Block diagram for vector control for GSC

B. Control Machine Side Converter Controller

The main purpose of control machine side converter (CMSC) controller is to synchronize the electrical output of the BDFTSIG with the grid. After the synchronization process the magnitude of both active and reactive power can be controlled via i_{qsc} and i_{dsc} current components respectively of the CM. The reference current components signals i_{qsc}^* and i_{dsc}^* are compared with the actual current components signals i_{qsc} and i_{dsc}, the errors are processed through a PI controller generating the CM stator voltage component signals v_{qsc} and v_{dsc} respectively, Then these voltages are compared with the compensation voltages v_{dsc}' and v_{qsc}' to obtain the reference voltages v_{dsc}^* and $v_{qsc}^*$of the PWM controlled IGBT bridge. The equations below offer a decoupled control.

Published By:
Blue Eyes Intelligence Engineering
and Sciences Publication (BEIESP)
© Copyright: All rights reserved.

The active and reactive power equations for the PM:

$$P_{sp} = \frac{3}{2}(v_{dsp}\, i_{dsp} + v_{qsp}\, i_{qsp}) \quad (23)$$

$$Q_{sp} = \frac{3}{2}(v_{qsp}\, i_{dsp} - v_{dsp}\, i_{qsp}) \quad (24)$$

Neglecting the stator resistance and by aligning the synchronously rotating *d*-axis reference frame with the stator voltage angle this will result in that the $v_{qs} = 0$ and since the amplitude of the supply voltage is constant, v_{ds} will be constant too, so the active and reactive power input to the stator of the PM in (23) & (24) can be rewritten in synchronously rotating *dq*-axis reference frame as follows:

$$P_{sp} = \frac{3}{2}\, v_{dsp}\, i_{dsp} \quad (25)$$

$$Q_{sp} = -\frac{3}{2}\, v_{dsp}\, i_{qsp} \quad (26)$$

Based on (25) & (26), the reactive power (Q_{sp}), can be controlled by the q-axis current of the PM (i_{qsp}), where the active power (P_{sp}), can be controlled by the d-axis current of the PM (i_{dsp}).

Fig. 5 shows the vector control of the BDFTSIG control system is implemented using Matlab/Simulink in synchronous rotating reference frame.

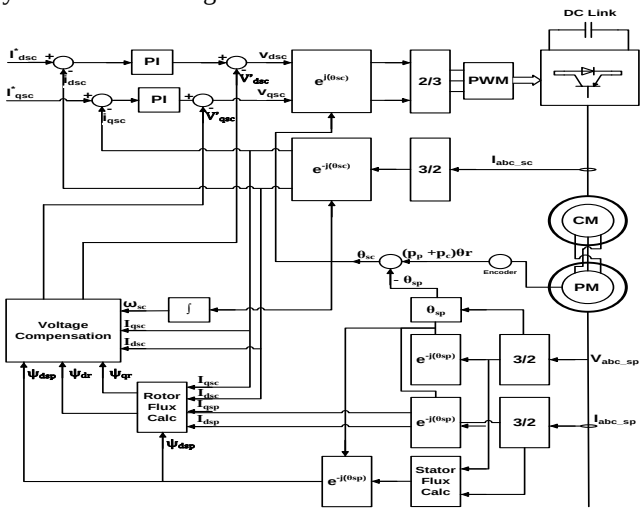

Fig. 5 Block diagram for vector control for CMSC

Grid synchronization:

The grid voltage component signals V_{dg} and V_{qg} are compared to the PM stator voltage component signals V_{dsp} and V_{qsp} respectively. The resulting error is processed by the PI controller producing the reference the CM stator current component signals $I^*_{dsc\_sync}$ and $I^*_{qsc\_sync}$. The current control signals control the excitation flux of the CM which is connected to the PM electrically through the rotor circuit controlling the excitation flux of the PM and hence the stator voltage magnitude and frequency.

Active & Reactive power control:

The active power control is achieved by regulating the PM stator d-axis current component i_{dsp} as shown in (25), this current component is regulated through the CM stator q-axis current component i_{qsc}. The available mechanical wind power is given by:

$$P_{wind} = \frac{1}{2}\rho\, A_T\, C_p(\lambda) V^3_{wind} \quad (27)$$

$$\lambda = \frac{\omega_T\, R_T}{V_{wind}} \quad (28)$$

$$C_p(\lambda) = 0.22\,(\frac{116}{\lambda_i} - 5)e^{-12.5/\lambda_i} \quad (29)$$

$$\frac{1}{\lambda_i} = \frac{1}{\lambda} - 0.03 \quad (61)$$

$$P_{Wind\ opt} = K_{opt}\, \omega_T^3 \quad (30)$$

For a gear ratio of 1:5, the power input to the generator at the generator speed is given by:

$$P_{Wind\ opt} = K'_{opt}\omega_g{}^3 \quad (31)$$

$$K'_{opt} = {}^1/_{5^3}\ K_{opt} \quad (32)$$

The constant K'_{opt} can be selected to extract the desired maximum wind power from the wind and this is done by controlling the active power of the system to achieve the optimum tip speed ratio (λ) and the coefficient of performance $C_p(\lambda)$ for a preset generator speed, for an optimum performance, the reactive power control is also controlled by regulating the PM stator q-axis current component i_{qsp} as shown in (26) this current component is regulated through the CM stator d-axis current component i_{dsc} to achieve the desired power factor.

IV. SIMULATION RESULTS

The system shown in fig. 1 is simulated and validated in Matlab/Simulink environment. The parameters shown in table 1 are for BDFTSIG, each machine is of rated power 4kW, 380V, 9.5A and 1500rpm, the parameters are referred to stator side, and the BDFTSIG system is driven at different reference speeds of 650 rpm sub-synchronous speed and at 850 rpm hyper-synchronous speed for different loading conditions. The wind turbine rated power is 5.5kW and the parameters are shown in table 2. The GSC was designed to regulate the DC link voltage at 150V with a 1000μF DC link capacitor, and a supply impedance of 0.1Ω resistance and 15mH inductance.

Published By:
Blue Eyes Intelligence Engineering
and Sciences Publication (BEIESP)
© Copyright: All rights reserved.

Table 1 Parameters of BDFTSIG

R_s [Ω]	R_r [Ω]	L_{ls}[H]	L_{lr}[H]	L_m[H]	p_p	p_c
1.405	1.395	0.006	0.006	0.172	2	2

Table 2 Parameters of wind turbine

R_T [m]	A_T [m^2]	Cut in speed[m/s]	Cut out speed[m/s]
3.1	30.2	2.5	11

A. GSC Simulation Results

Fig. 6 shows the simulation result with i_{qg}^* set to zero (unity pf). The phase voltage and current are in phase.

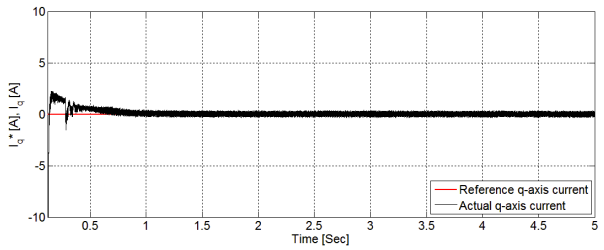

(a)

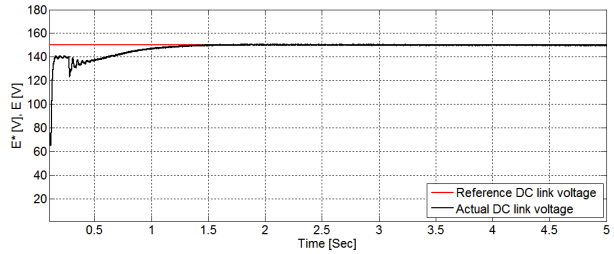

(b)

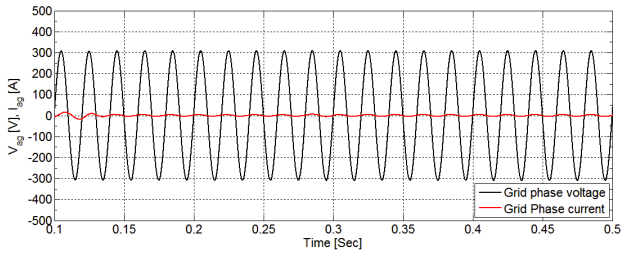

(c)

Fig. 6 GSC simulation results at unity pf: (a) q-axis current component, (b) DC-link voltage, (c) Phase voltage and current

B. Synchronization Simulation Results

Fig. 7 show the simulation results of the phase voltages for both the grid and PM stator wave forms, also the controlled grid & PM stator voltages in dq synchronous rotating reference frame during the synchronization process which takes 0-0.1 sec till the synchronization ends.

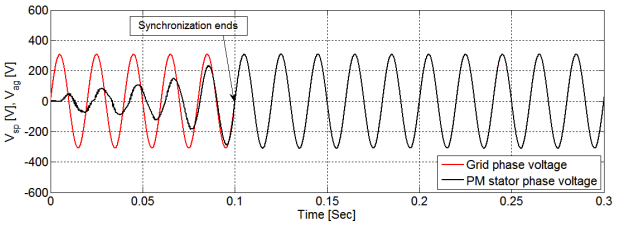

(a)

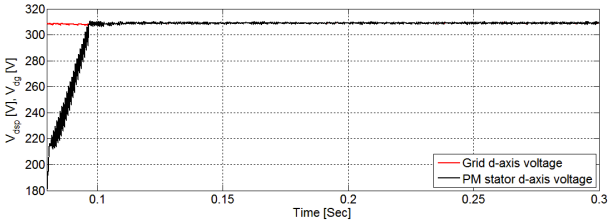

(b)

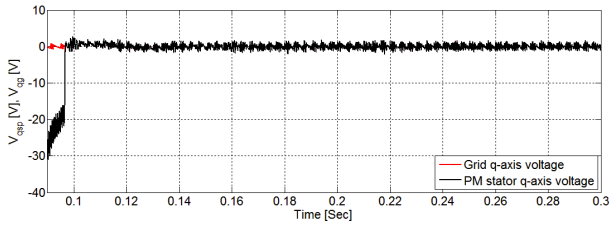

(c)

Fig. 7 PM Stator dq-axis components during synchronization: (a) Grid and PM phase voltages during synchronization, (b) d-axis voltage, & (c) q-axis voltage.

C. Active & Reactive Power Control Simulation Results

Fig. 8 (a) shows that the PM stator active power at 650rpm, which is regulated at 2200W; Fig. 8 (b) shows that the CM stator absorbs 670W from the grid. Fig. 8 (c) shows the system mechanical power input of 2150W. The efficiency of the system is almost 70%. Fig. 9 (a) shows that the PM stator active power at 850rpm, which is regulated at 3800W; Fig. 9 (b) shows that the CM stator power supplies 170W to the grid. Fig. 9 (c) shows the system mechanical power input of 5050W. The efficiency of the system is almost 78%. In all the cases the gear box losses are neglected.

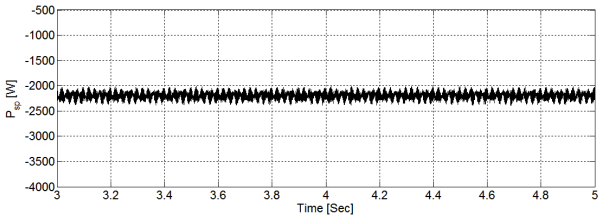

(a)

Published By:
Blue Eyes Intelligence Engineering
and Sciences Publication (BEIESP)
© Copyright: All rights reserved.

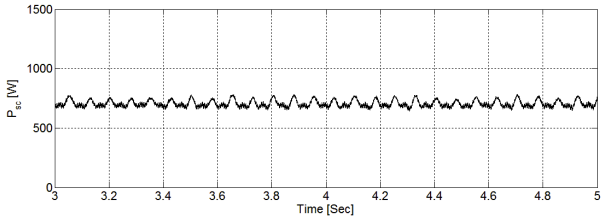

(b)

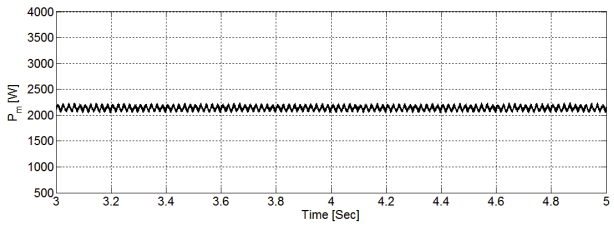

(c)

Fig. 8 Simulation results at 650rpm: (a) PM Stator active power, (b) CM Stator active power, (c) Mechanical power input

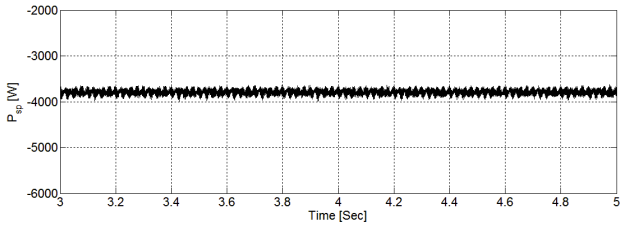

(a)

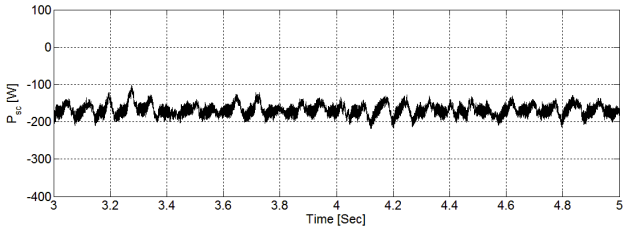

(b)

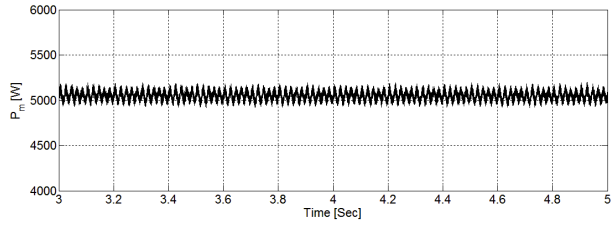

(c)

Fig. 9 Simulation results at 850rpm: (a) PM Stator active power, (b) CM Stator active power, (c) Mechanical power input

Fig. 10 shows the simulation results of the steady state BDFTSIG efficiency at different rotor speeds of 650 and 850rpm for varying loading conditions of 2200 and 3800W respectively extracted at PM stator terminals.

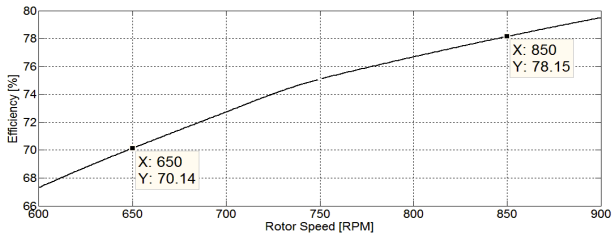

Fig. 10 BDFTSIG efficiency

Fig. 11 shows the simulation results of the BDFTSIG at different rotor speeds of 650 and 850rpm for a varying loading with additional load connected at in the instant 5s.

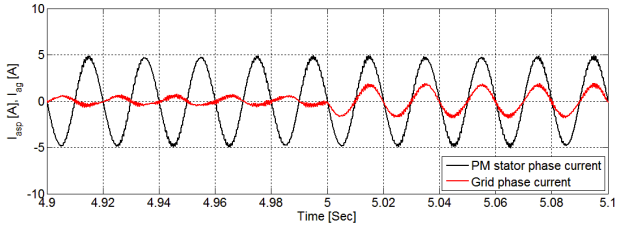

(a)

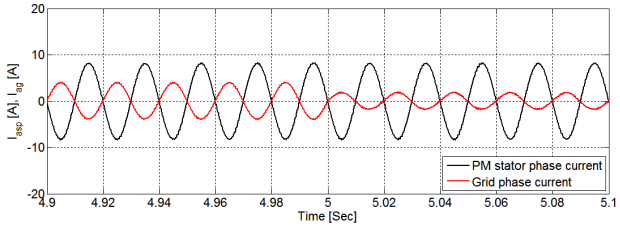

(b)

Fig. 11 PM Stator and grid phase currents: (a) at 650 rpm, (b) at 850 rpm.

Figs. 12-13 show the simulation results for CM stator dq current components, PM stator dq current components, and PM stator active and reactive power, due to a step d-axis current component reference input at rotor speeds of 650 and 850 rpm, these figures show the decoupled control of both active and reactive power components, there is a slightly coupling effect, causing a slight change on the active power component.

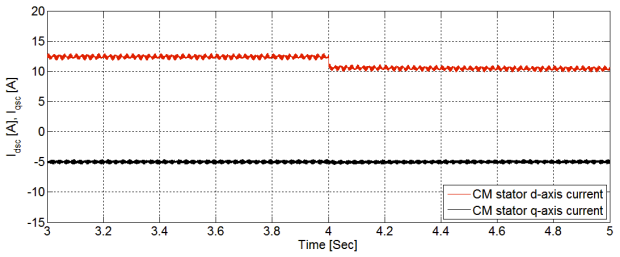

(a)

Published By:
Blue Eyes Intelligence Engineering and Sciences Publication (BEIESP)
© Copyright: All rights reserved.

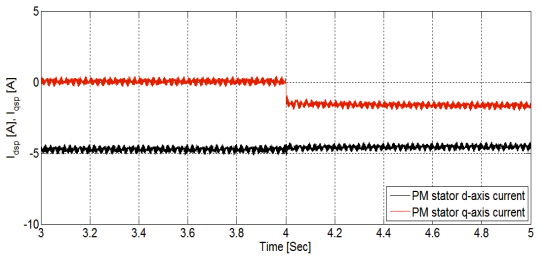

(b)

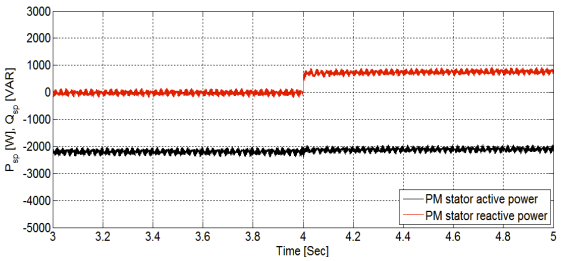

(c)

Fig. 12 Simulation results @ 650 rpm. (a) CM Stator dq currents, (b) PM Stator dq currents, (c) PM Active and reactive power

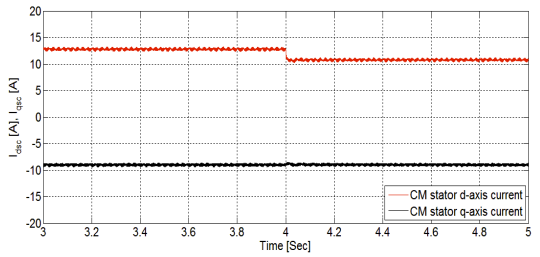

(a)

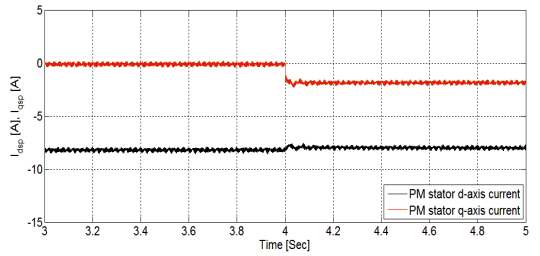

(b)

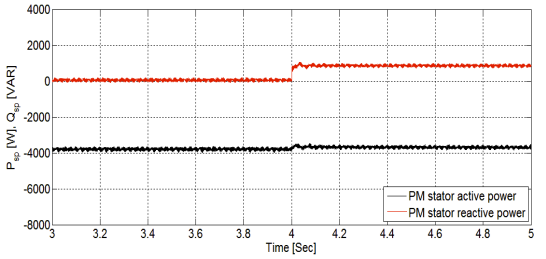

(c)

Fig. 13 Simulation results @ 850 rpm. CM Stator dq currents, (b) PM Stator dq currents, (c) PM Active and reactive power

V. CONCLUSION

A steady state and dynamic modeling for inversely connected rotor of a BDFTSIG with vector control for both grid side and control machine side converters have been presented in this paper. The vector control scheme of GSC for controlling the DC link voltage was achieved regardless the power flow though the CM stator terminals, also the synchronization process was achieved in a fast and smooth way, matching the amplitude, frequency and phase of the PM stator voltage with the grid voltages, it assured the conditions for the synchronization through controlling the CM stator current components, also the vector control scheme of CMSC for controlling both the active and reactive power of the PM stator was validated, the power factor at the PM stator was improved. The vector control scheme of the inversely connected rotor of BDFTSIG system was robust and the simulation results showed a good transient performance under variable loading, power factor settings and rotor speed conditions. The only disadvantage is the efficiency of the BDFTSIG which can be compensated by the lower maintenance cost by the elimination of slip rings and carbon brushes and also by increasing the reliability and availability of the wind turbine system. Finally The inversely connected rotor of a BDFTSIG proves to be a good alternative for DFIG.

REFERENCES

1. U. Shipurkar. H. Polinder, J.A. Ferreira, “A Review of Methods to Increase the Availability of Wind Turbine Generator Systems”, CPSS Transactions on power electronics and applications, Vol. 1, No. 1, Dec. 2016, pp. 66-82.
2. R. Bia, K. Qianb, C. Zhoua, D. M. Hepburna, J. Rong, “ A survey of failures in wind turbine generator systems with focus on a wind farm in China”, International Journal of Smart Grid and Clean Energy, Vol. 3, No. 4, Oct. 2014. pp. 366-373.
3. K. Fischer, F. Besnard, L. Bertling, “Reliability-Centred Maintenance for Wind Turbines Based on Statistical Analysis and Practical Experience”, IEEE Transactions on Energy Conversion, Vol.27, Issue: 1, March 2012, pp. 184-195.
4. P.C. Roberts, R.A. McMahon, P.J. Tavner, J.M. Maciejowski, T.J. Flack, X. Wang, “Performance of Rotors in a Brushless Doubly-Fed Induction Machine (BDFM)”, Proc. 16th Int. Conf. Electrical machines, Cracow, Poland, 2004, pp. 450–455.
5. P.C. Roberts, R.A. McMahon, P.J. Tavner, J.M. Maciejowski and T.J. Flack,“Equivalent circuit for the brushless doubly fed machine (BDFM) including parameter estimation and experimental verification”, IEE Proc.-Electr. Power Appl., Vol. 152, No. 4, 2005, pp. 933-942.
6. F. Blazquez, C. Veganzones, D. Ramirez, and C. Platero, “Characterization of the Rotor Magnetic Field in a Brushless Doubly-Fed Induction Machine”, IEEE Transactions on Energy Conversion, Vol. 24, No. 3, 2009, pp. 599-607.
7. S. M. Allam, A. M. Azmy, and M. A. El-Khazendar, “A General Model for Describing the Performance of Brushless Doubly-Fed Induction Machines”, The Journal of Engineering Research, Vol. 7, No. 2, 2010, pp. 1-9.
8. Hamed Gorginpour1, Hashem Oraee, Richard A. McMahon, “Performance Description of Brushless Doubly-Fed Induction Machine in Its Asynchronous and Variable Speed Synchronous Modes”, Journal of Electromagnetic Analysis and Applications, Vol. 3, 2011, pp. 490-511.
9. M. N. Hashemnia and F. Tahami,“Steady State Analysis of Brushless Doubly Induction Machine Taking Core Loss into Account”, 38th Annual Conference on IEEE Industrial Electronics Society, 2012, pp. 2030-2035.
10. Duro Basic, Jian Guo Zhu, and Gerard Boardman, “Transient Performance Study of a Brushless Doubly Fed Twin Stator Induction Generator”, IEEE Transactions on Energy Conversion, Vol. 18, No. 3, 2003, pp. 400-408.

Published By:
Blue Eyes Intelligence Engineering
and Sciences Publication (BEIESP)
© Copyright: All rights reserved.

11. Basic Duro, Zhu Jianguo, and Boardman Gerard, "Modeling and steady state performance analysis of brushless doubly fed twin stator induction generator", Australian Power engineering Committee, Monash Univ. Melbourne, Australia, 2002, pp. 6.
12. Marek Adamowicz, Ryszard Strzelecki, and Daniel Wojciechowski, "Steady State Analysis of Twin Stator Cascaded Doubly Fed Induction Generator", Compatibility in Power Electronics, 2007, pp. 1-5.
13. Zoheir Tir, Hammoud Rajeai, and Rachid Abdessemed, "Analysis and vector control of a cascaded doubly fed induction generator in wind energy applications", Revue des Energies Renouvelables , SMEE'10 Bou Ismail Tipaza, 2010, pp. 347 – 358.
14. Kostyantyn Protsenko and Dewei Xu,, "Modeling and Control of Brushless Doubly-FedInduction Generators in Wind Energy Applications", IEEE Transactions on Power Electronics, VOL. 23, No. 3, 2008, pp. 1191-1197.
15. Bensadeq, P. W. Lefley, "Design and Control of the Brushless Doubly Fed Twin Induction Generator (BDFTIG)", 14th International Power Electronics and Motion Control Conference, 2010, pp. 72-76.
16. R. Pena, J.C. Clare, and G.M. Asher, "A doubly fed induction generator using back to back PWM converters supplying an isolated load from variable speed wind turbine", IEE Proc.-Electr. Power Appl. Vol. I43, No. 5, 1996, pp. 380-387.
17. R. Pena, J.C. Clare, and G.M. Asher,"Doubly fed induction generator using back-to-back PWM converters and its application to variable speed wind-energy generation", IEE Proc.-Electr. Power Appl. Vol. I43, No. 5, 1996, pp. 231-241.
18. Wei Qiao,"Dynamic Modeling and Control of Doubly Fed Induction Generators Driven by Wind Turbines", IEEE/PES Power Systems Conference and Exposition, 2009, pp. 1-8.
19. Gilsung Byeon, In Kwon Park, and Gilsoo Jang, "Modeling and Control of a Doubly-Fed Induction Generator (DFIG) Wind Power Generation System for Real-time Simulations", Journal of Electrical Engineering & Technology Vol. 5, No. 1, 2010, pp. 61-69.
20. Riyadh Rouabhi, Rachid Abdessemed, Aissa Chouder, Ali Djerioui, "Power Quality Enhancement of Grid Connected Doubly-Fed Induction Generator Using Sliding Mode Control", International Review of Electrical Engineering (I.R.E.E.), Vol. 10, No. 2, 2015, pp. 266-276

APPENDIX

A. Dynamic model of BDGTSIG derivation:

The stator voltage equations for PM:

$$V_{qsp} = R_{sp}\, i_{qsp} + \frac{d}{dt}\psi_{qsp} + \omega_{sp}\,\psi_{dsp} \quad (A.1)$$

$$V_{dsp} = R_{sp}\, i_{dsp} + \frac{d}{dt}\psi_{dsp} - \omega_{sp}\,\psi_{qsp} \quad (A.2)$$

The rotor voltage equations for PM:

$$V_{qrp} = R_{rp}\, i_{qrp} + \frac{d}{dt}\psi_{qrp} + (\omega_{sp} - p_p\omega_m)\,\psi_{drp} \quad (A.3)$$

$$V_{drp} = R_{rp}\, i_{drp} + \frac{d}{dt}\psi_{drp} - (\omega_{sp} - p_p\omega_m)\,\psi_{qrp} \quad (A4)$$

Flux linkage equations:

$$\psi_{qsp} = L_{lsp}i_{qsp} + L_{mp}\left(i_{qsp} + i_{qrp}\right) \quad (A.5)$$
$$\psi_{dsp} = L_{lsp}i_{dsp} + L_{mp}\left(i_{dsp} + i_{drp}\right) \quad (A.6)$$
$$\psi_{qrp} = L_{lrp}i_{qrp} + L_{mp}\left(i_{qrp} + i_{qsp}\right) \quad (A.7)$$
$$\psi_{drp} = L_{lrp}i_{drp} + L_{mp}\left(i_{drp} + i_{dsp}\right) \quad (A.8)$$

Now, rewriting the stator and rotor voltage equations (A1 – A3) after substituting with the flux linkage (A.5 – A.8)

$$V_{qsp} = \left(R_{sp} + sL_{sp}\right)i_{qsp} + \omega_{sp}L_{sp}i_{dsp} + sL_{mp}i_{qrp} + \omega_{sp}L_{mp}i_{drp} \quad (A.9)$$

$$V_{dsp} = -\omega_{sp}L_{sp}i_{qsp} + \left(R_{sp} + sL_{sp}\right)i_{dsp} - \omega_{sp}L_{mp}i_{qrp} + sL_{mp}i_{drp} \quad (A.10)$$

Where $s = {}^{d}/_{dt}$,

$$V_{qrp} = sL_{mp}i_{qsp} + \left(\omega_{sp} - p_p\omega_m\right)L_{mp}i_{dsp} + \left(R_{rp} + sL_{rp}\right)i_{qrp} + \left(\omega_{sp} - p_p\omega_m\right)L_{rp}i_{drp} \quad (A.11)$$

$$V_{drp} = -\left(\omega_{sp} - p_p\omega_m\right)L_{mp}i_{qsp} + sL_{mp}i_{dsp} - \left(\omega_{sp} - p_p\omega_m\right)L_{rp}i_{qrp} + \left(R_{rp} + sL_{rp}\right)i_{drp} \quad (A.12)$$

The stator and rotor voltage equations for CM:

$$V_{qsc} = (R_{sc} + sL_{sc})i_{qsc} + \omega_{sc}L_{sc}i_{dsc} + sL_{mc}i_{qrc} + \omega_{sc}L_{mc}i_{drc} \quad (A.13)$$

$$V_{dsc} = -\omega_{sc}L_{sc}i_{qsc} + (R_{sc} + sL_{sc})i_{dsc} - \omega_{sc}L_{mc}i_{qrc} + sL_{mc}i_{drc} \quad (A.14)$$

$$V_{qrc} = sL_{mc}i_{qsc} + (\omega_{sc} - p_c\omega_m)L_{mc}i_{dsc} + (R_{rc} + sL_{rc})i_{qrc} + (\omega_{sc} - p_c\omega_m)L_{rc}i_{drc} \quad (A.15)$$

$$V_{drc} = -(\omega_{sc} - p_c\omega_m)L_{mc}i_{qsc} + sL_{mc}i_{dsc} - (\omega_{sc} - p_c\omega_m)L_{rc}i_{qrc} + (R_{rc} + sL_{rc})i_{drc} \quad (A.16)$$

According to the *inversely sequence* rotor connection between the PM & CM, the electrical quantities has the following relationships:

Rotor voltages and currents relations:

$$V_{qrp} = V_{qrc} \quad (A.17)$$
$$V_{drp} = -V_{drc} \quad (A.18)$$
$$i_{qrp} = -i_{qrc} = i_{qr} \quad (A.19)$$
$$i_{drp} = i_{drc} = i_{dr} \quad (A.20)$$

From (A.17), (A.11), (A.15), (7), (A.19) and (A.20)

$$sL_{mp}i_{qsp} + \left(\omega_{sp} - p_p\omega_m\right)L_{mp}i_{dsp} + (R_r + sL_r)i_{qrp} + \left(\omega_{sp} - p_p\omega_m\right)L_r i_{drp} - sL_{mc}i_{qsc} + \left(\omega_{sp} - p_p\omega_m\right)L_{mc}i_{dsc} = 0 \quad (A.21)$$

From (A.18), (A.12), (A.16), (7), (A.19) and (A.20)

$$-\left(\omega_{sp} - p_p\omega_m\right)L_{mp}i_{qsp} + sL_{mp}i_{dsp} - \left(\omega_{sp} - p_p\omega_m\right)L_r i_{qrp} + (R_r + sL_r)i_{drp} + \left(\omega_{sp} - p_p\omega_m\right)L_{mc}i_{qsc} + sL_{mc}i_{dsc} = 0 \quad (A.22)$$

From (A.13), (A.14), (7), (A.19) and (A.20)

$$V_{qsc} = -sL_{mc}i_{qrp} + \left(\left(p_p + p_p\right)\omega_m - \omega_{sp}\right)L_{mc}i_{drp} + (R_{sc} + sL_{sc})i_{qsc} + \left(\left(p_p + p_p\right)\omega_m - \omega_{sp}\right)L_{sc}i_{dsc} \quad (A.23)$$

$$V_{dsc} = \left(\left(p_p + p_p\right)\omega_m - \omega_{sp}\right)L_{mc}i_{qrp} + sL_{mc}i_{drp} - \left(\left(p_p + p_p\right)\omega_m - \omega_{sp}\right)L_{sc}i_{qsc} + (R_{sc} + sL_{sc})i_{dsc} \quad (A.24)$$

Published By:
Blue Eyes Intelligence Engineering
and Sciences Publication (BEIESP)
© Copyright: All rights reserved.